Computing Systems in Engineering Vol. 1, Nos 2–4, pp. 237–256, 1990
Printed in Great Britain.

0956-0521/90 $3.00+0.00
Pergamon Press plc

ENSAERO—A MULTIDISCIPLINARY PROGRAM FOR FLUID/STRUCTURAL INTERACTION STUDIES OF AEROSPACE VEHICLES

G. P. GURUSWAMY

Applied Computational Fluids Branch, NASA Ames Research Center, Moffett Field, CA 94035, U.S.A.

(*Received* 20 *April* 1990)

Abstract—Strong interactions can occur between the flow about an aerospace vehicle and its structural components, resulting in several important aeroelastic phenomena. These aeroelastic phenomena can significantly influence the performance of the vehicle. At present, closed-form solutions are available for aeroelastic computations when flows are in either the linear subsonic or supersonic range. However, for aeroelasticity involving complex nonlinear flows with shock waves, vortices, flow separations, and aerodynamic heating, computational methods are still under development. These complex aeroelastic interactions can be dangerous and limit the performance of aircraft. Examples of these detrimental effects are aircraft with highly swept wings experiencing vortex-induced aeroelastic oscillations, a transonic regime at which the flutter speed is low, aerothermoelastic loads that play a critical role in the design of high-speed vehicles, and flow separations that often lead to buffeting with undesirable structural oscillations. The simulation of these complex aeroelastic phenomena requires an integrated analysis of fluids and structures. A summary is provided of the development of a multidisciplinary computational tool based on the Euler/Navier–Stokes flow equations and finite element structural equations, and their applications to aeroelasticity.

INTRODUCTION

The understanding of the nature of flows and their interactions with structures is becoming increasingly important for aerospace vehicles. High performance and maneuverability are playing major roles in design. Flows over fighters at high angles of attack are quite often complex, and are associated with vortices and shock waves. Formation of vortices changes the aerodynamic load distribution on a wing. Vortices formed on aircraft have caused several instabilities, such as aeroelastic oscillations for a highly swept flexible wing.[1,2] In the transonic regime, aircraft experience low flutter speeds due to moving shock waves.[3,4] Such instabilities can severely impair the performance of an aircraft. On the other hand, there are possibilities of using the vortices to control aircraft at high angles of attack when some of the conventional control techniques are not adequate. Advanced methods, such as active controls, are being developed to control the aircraft aeroelastic oscillations. Strong interactions between fluids and structures occur through the control surfaces.[5,6] In addition, thermal loads can further complicate such interactions for high-speed vehicles such as hypersonic aircraft.[7]

For accurate computation of flows and inclusion of interactions with structures, it is necessary to solve the Navier–Stokes equations and couple them with the structural equations. Recently, methods were developed to accurately couple the Euler[8] and Navier–Stokes[9] solutions with the structural equations, and they are incorporated in a multidisciplinary aeroelastic code, ENSAERO. This new code computes aeroelastic responses by simultaneously integrating the Euler/Navier–Stokes equations and the structural equations of motion using aeroelastically adaptive dynamic grids. The flow is solved by time-accurate finite difference schemes based on the Beam–Warming algorithm.[10,11] The code was used to make computations for flexible wings to demonstrate the effects of vortical flows.[9]

In this paper, a procedure for multidisciplinary computations of flow/structure interaction problems of flexible aerospace vehicles is presented. This work is a part of a larger effort within the Applied Computational Fluids Branch of Ames Research Center to further develop ENSAERO as an efficient multidisciplinary code to compute flows over aerospace vehicles, including thermal loads and active controls. The flow equations are based on the Euler/Navier–Stokes equations. This new code is being designed in a modular fashion to adapt several different numerical schemes suitable for accurate aeroelastic computations. The candidate flow solvers are based on schemes such as central difference schemes with artificial viscosity,[11] the streamwise upwind schemes,[12] etc. The basic coding accommodates zonal grid techniques for efficient modeling of full aircraft.[13] This computational capability is also being designed in such a way that finite elements can be directly used for more complete modeling of structures. This will be an improvement over the modal approach that is currently used. Several multidisciplinary modules such as active controls, thermo-elastic displacements, etc. are being implemented.

This paper describes the procedure of coupling the flow solutions with the structural equations of motion, including active controls and thermal loads. Results are demonstrated for aeroelastic responses of wings with vortical flows on typical fighter wings.

GOVERNING AERODYNAMICS EQUATIONS

The strong conservation law forms of the Navier–Stokes equations are used for shock-capturing purposes. The equations in Cartesian coordinates in nondimensional form can be written as

$$\frac{\partial Q}{\partial t}+\frac{\partial E}{\partial x}+\frac{\partial F}{\partial y}+\frac{\partial G}{\partial z}=\frac{\partial E_v}{\partial x}+\frac{\partial F_v}{\partial y}+\frac{\partial G_v}{\partial z}. \tag{1}$$

To enhance numerical accuracy and efficiency and to handle boundary conditions more easily, the governing equations are transformed from the Cartesian coordinates to general curvilinear coordinates, where

$$\begin{aligned}\tau &= t\\ \xi &= \xi(x, y, z, t)\\ \eta &= \eta(x, y, z, t)\\ \zeta &= \zeta(x, y, z, t).\end{aligned} \tag{2}$$

The resulting transformed equations are not much more complicated than the original Cartesian set and can be written in nondimensional form as

$$\frac{\partial}{\partial\tau}\hat{Q}+\frac{\partial}{\partial\xi}(\hat{E}-\hat{E}_v)+\frac{\partial}{\partial\eta}(\hat{F}-\hat{F}_v)+\frac{\partial}{\partial\zeta}(\hat{G}-\hat{G}_v)=0, \tag{3}$$

where $\hat{}$ indicates the transformed quantities.

In order to solve Eq. (3) for the full flow, a very fine grid throughout the flow field is required. In high Reynolds number flows, the viscous effects are confined to a thin layer near rigid boundaries. In most practical cases, because of computer storage and speed limitations, there are only enough grid points to resolve the gradients normal to the body by clustering the grid in the normal direction, and resolution along the body is similar to what is needed in inviscid flow calculations. As a result, even though the full derivatives are retained in the equations, the gradients along the body are not resolved unless the streamwise and circumferential grid spacings are sufficiently small. Hence, for many Navier–Stokes computations, the viscous derivatives along the body are dropped. This leads to the thin-layer Navier–Stokes equations. In this paper, the thin-layer Navier–Stokes form of Eq. (3) is used for modeling the flow.

The thin-layer model requires a boundary-layer-type coordinate system. In our case, the ξ and η directions are along the body and the viscous derivatives associated with these directions are dropped, whereas the terms in ζ are retained and the body surface is mapped onto a constant ζ surface. Thus, Eq. (3) simplifies to

$$\partial_\tau\hat{Q}+\partial_\xi\hat{E}+\partial_\eta\hat{F}+\partial_\zeta\hat{G}=\mathrm{Re}^{-1}\,\partial_\zeta\hat{S}. \tag{4}$$

It should be emphasized that the thin-layer approximation is valid only for high Reynolds number flows. Also, very large turbulent eddy viscosities invalidate the model.

AERODYNAMICS SOLUTION PROCEDURES

Computational efficiency is a major requirement in selecting solution procedures. In the multidisciplinary computations, the solution of aerodynamic equations requires about 50% of the computational time. As a result, numerical efficiency of the aerodynamic solution procedure is an important factor in the multidisciplinary code development.

Several numerical schemes have been developed to solve Eq. (4). To date, one of the well tested schemes is the implicit approximate factorization algorithm of Beam and Warming[10] based on the central differencing. The diagonal implicit form of the Beam–Warming method reported by Pulliam and Chaussee[11] has further reduced the computational time. The central difference schemes require specification of an artificial dissipation to stabilize the computations. Often such artificial dissipations lead to dissipative solutions. In order to overcome this deficiency of central difference schemes, upwind schemes were developed. To date most of the upwind schemes are based on flux-splitting in the coordinate direction. Recently, Obayashi and Goorjian[12] have developed a new upwind scheme based on flux-splitting in the streamwise direction. This new streamwise upwind scheme computes flows more accurately than the coordinate-direction upwind schemes.

The current version of ENSAERO has both options of central differencing and streamwise upwinding. Both methods are equally efficient in computational speed.

One of the main bottlenecks in using the Navier–Stokes equations is the lack of proper turbulence modeling. Solving turbulent flows directly without modeling the turbulence is a very difficult task because of the extreme time and space scales associated with turbulent motion. Hence, to date, the most common method of simulating turbulent flows is through an approximate turbulence model that is implemented into the Reynolds-averaged Navier–Stokes equations. In this work the turbulence model proposed by Baldwin and Lomax[14] is used.

AEROELASTIC EQUATIONS OF MOTION

The governing aeroelastic equations of motion of a flexible wing are solved using the Rayleigh–Ritz method. In this method, the resulting aeroelastic displacements at any time are expressed as a function of a finite set of assumed modes. The contribution of

each assumed mode to the total motion is derived by Lagrange's equation. Furthermore, it is assumed that the deformation of the continuous wing structure can be represented by deflections at a set of discrete points. This assumption facilitates the use of discrete structural data, such as the modal vector, the modal stiffness matrix, and the modal mass matrix. These can be generated from a finite-element analysis or from experimental influence-coefficient measurements. In this study, the finite-element method is used to obtain the modal data.

It is assumed that the deformed shape of the wing can be represented by a set of discrete displacements at selected nodes. From the modal analysis, the displacement vector $\{d\}$ can be expressed as

$$\{d\} = [\phi]\{q\}, \tag{5}$$

where $[\phi]$ is the modal matrix and $\{q\}$ is the generalized displacement vector. The final matrix form of the aeroelastic equations of motion is

$$[M]\{\ddot{q}\} + [G]\{\dot{q}\} + [K]\{q\} = \{F\}, \tag{6}$$

where $[M]$, $[G]$, and $[K]$ are modal mass, damping, and stiffness matrices, respectively. $\{F\}$ is the aerodynamic force vector, defined as $(\frac{1}{2})\rho U_\infty^2 [\phi]^T [A]\{\Delta C_p\}$, and $[A]$ is the diagonal area matrix of the aerodynamic control points.

The aeroelastic equation of motion, Eq. (6), is solved by a numerical integration technique based on the linear acceleration method.[15]

FINITE ELEMENT STRUCTURES

The finite element is a well developed technology for solving structural problems. General-purpose codes based on the finite element methods, such as NASTRAN, are available for analyzing structures coupled with linear aerodynamics. On the other hand, for the solution of nonlinear flow problems, finite element methods are still in their early stages of development when compared to finite-difference methods. For ENSAERO, finite differences are used for flows and finite elements for structures. The coupling between two methods is achieved by interpolations. Modes generated by a rectangular element available in the code are shown in Fig. 1.

One of the purposes of this work is to conduct aerothermoelastic analysis of aerospace vehicles such as NASP. The finite elements used in the present development can model the thermal loads. It is assumed that the temperature distribution is given by the aerodynamic equations. To treat thermal loads, the analysis method is divided into two steps. First, assuming that all nodal points are restrained, the stresses developed within all elements due to temperature changes are found. Next the element corner forces that maintain these stresses are obtained. Then, to eliminate these corner forces, the system is analyzed for nodal point loads which are equal in magnitude but opposite in sign to these restraining forces. These nodal forces are added to the aerodynamic loads. More details can be found in books such as Ref. 16. A procedure of modeling the thermal loads in a finite element program is illustrated by the present author in Ch. 13 of Ref. 16.

Equations similar to Eq. (6) can be solved using the direct matrices from the finite element method in place of the modal matrices. The thermal loads can be added to the right hand side of Eq. (6).

ACTIVE CONTROL SURFACES

Many physically important phenomena occur in engineering because of strong coupled interactions between structures and fluids. One such case is the use of wings with active control surfaces. Aerodynamic means can be developed through active controls to counter the forces and moments that drive flutter and dynamic instability. Use of active control is important for future aircraft, which will tend to be more flexible for high maneuverability.

Recently, a procedure for simulating the active coupling of structures and nonlinear flows was presented.[5] The approach is oriented towards synthesizing active controls of aeroelastically oscillating wings with unsteady transonics in the time domain. This procedure was implemented in the TSP code ATRAN3S[5] and the role of shock waves on active controls was studied. The scheme presented in this work is general in nature and can be extended to study engineering problems where structures and fluids are strongly coupled through some type of active control systems.

In the present work, a procedure similar to one available in ATRAN3S is implemented in ENSAERO. It is assumed that a control law is known from detailed control theory analysis for a given configuration. By using the present procedure the coupled phenomenon of structures, aerodynamics, and active controls can be accurately simulated. A typical control law in the time domain can be assumed as

$$\delta = G_1 h_1(t) e^{i\psi_1} + G_2 \alpha_1(t) e^{i\psi_2}, \tag{7}$$

where

δ	= control surface deflection
G_1, G_2	= gain factors
h_1	= deflection at a selected point on the wing
α_1	= angle of attack at a selected span station
ψ_1, ψ_2	= phase angles.

By representing the active control law in the above form, the coupled phenomenon of structures, aerodynamics, and active controls can be studied in a realistic time domain.

One major difference between ATRAN3S and

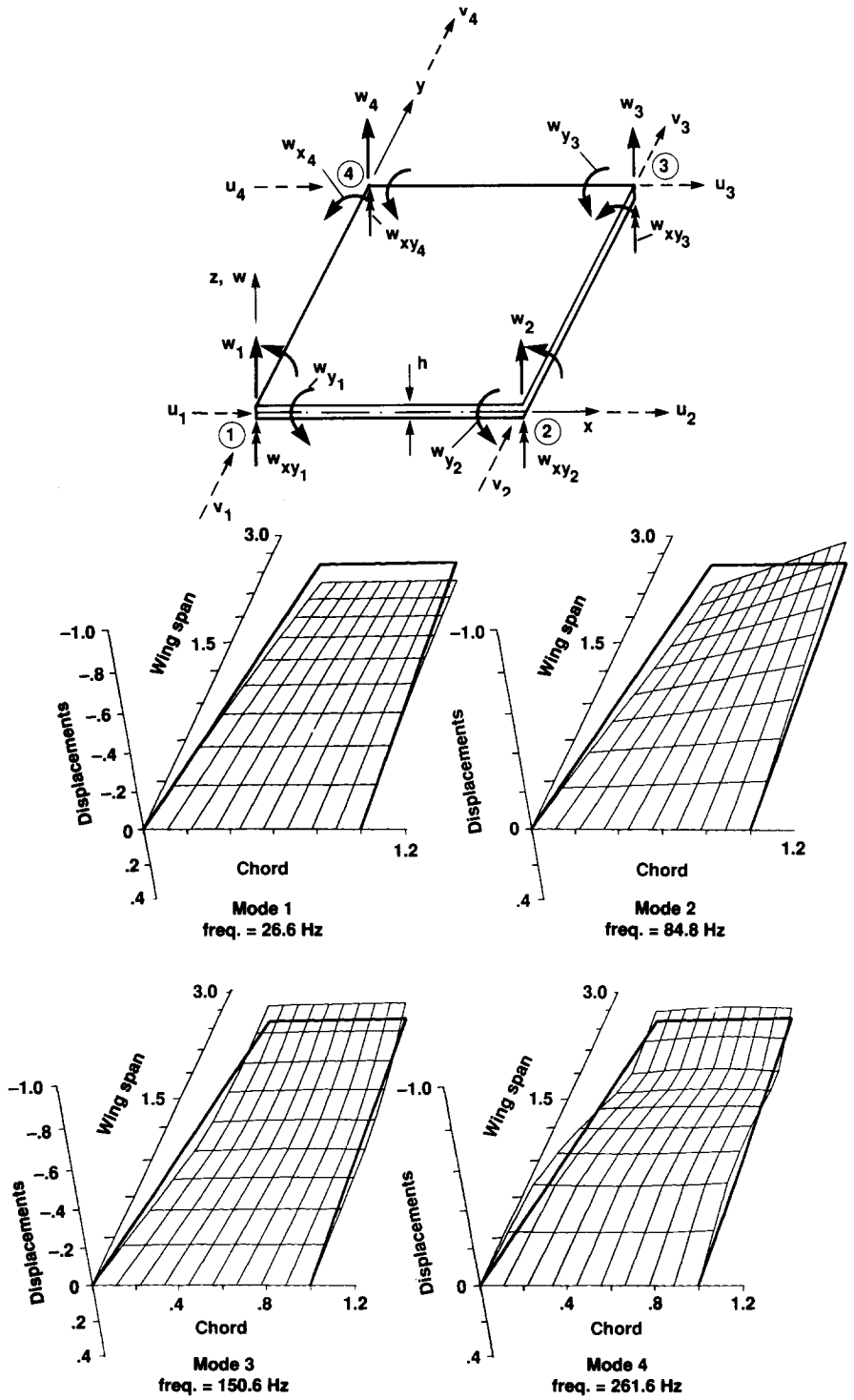

Fig. 1. Mode shapes and frequencies of a rectangular wing using the finite element method.

ENSAERO is in the grids. Grids are not moved in ATRAN3S for control surfaces because of the use of the small disturbance equations. Since ENSAERO uses Euler/Navier–Stokes equations, grids need to be moved according to the control surface movements. Currently, control surface deflections are modeled without moving the grid, and the flow boundary conditions are modified by using the small perturbation equations. This procedure is valid only for small control surface oscillations. A complete method which uses a sliding zonal-grid with shearing is under implementation.

CONFIGURATION-ADAPTIVE MOVING GRIDS

One of the major problems in computational aerodynamics using the Euler/Navier–Stokes equations lies in the area of grid generation. For the case of steady flows, advanced techniques such as zonal grids[14] are being used for full aircraft. Such a grid-generation technique for aeroelastic calculations involving moving components is developed for ENSAERO.[17] The effects of the aeroelastic-configuration-adaptive dynamic grids on the stability and accuracy of the numerical schemes are being studied in detail.

In this work, the zonal grid technology based on the work in Ref. 13 is implemented. Figure 2 illustrates a schematic approach to go from zonal grids in the physical space to the computational space. Figure 3 illustrates the overlapping of a fine grid with a coarse grid for a two-zone grid. In the current development this procedure is extended to moving grids.[17]

An important part of this dynamic grid system was the development of an algebraic grid-generation technique for aeroelastic applications. The algebraic method was selected to minimize the computational overhead caused by grid generation. For accurate aeroelastic computations, grids need to be generated at each time step. Such analytical methods as those based on solving the elliptic differential equations are computationally expensive.

The grid scheme in ENSAERO satisfies four general requirements for a successful grid, namely: (1) the grid lines intersect normal to the wing surface in the chordwise direction; (2) the grid cells are smoothly stretched away from the wing surface; (3) the outer boundaries are located far from the wing to minimize the effect of boundary reflections; and (4) the grids adapt to the deformed wing position at each time step.

The computational grids used for wings in this study have a C–H topology, as shown in Fig. 4 for a typical fighter wing. The grid deforms to remain coincident with the wing surface as it deflects, while the outer boundary of the grid is fixed in space. At the end of each time step, the deformed shape of the wing is computed using Eq. (5) including the control surface deflections given by Eq. (7). The ξ and η grid distributions on the grid surface corresponding to the wing surface (ζ grid index = 1) are obtained from previously assumed distributions. These distributions are selected to satisfy the general requirements of a grid for accurate computations. In this work, the grid in the ξ direction is selected so that the grid

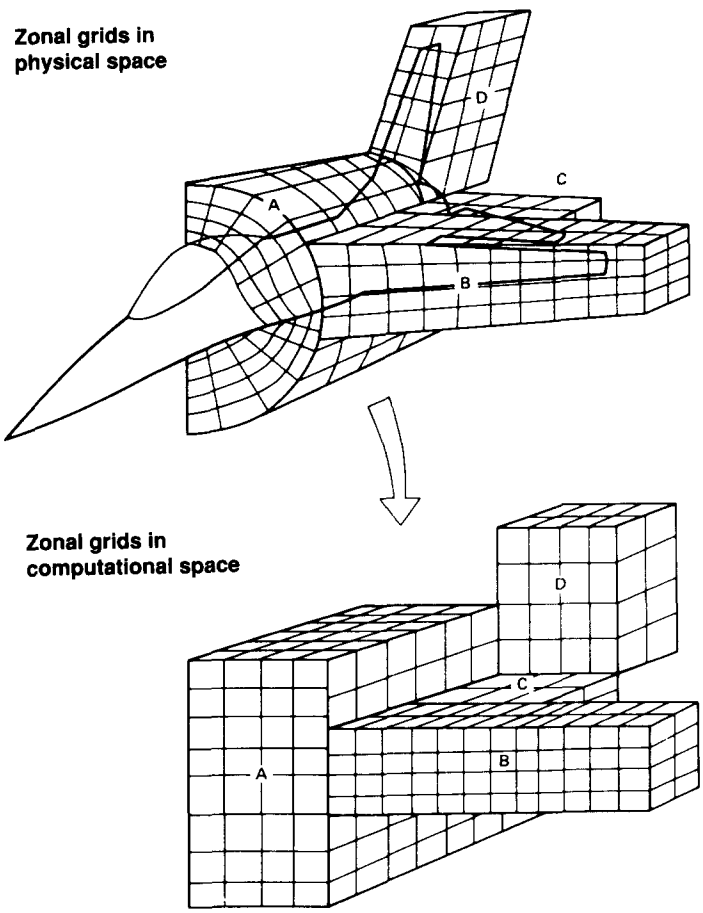

Fig. 2. Body-conforming zonal grids of a fighter aircraft configuration in the physical and computational space.

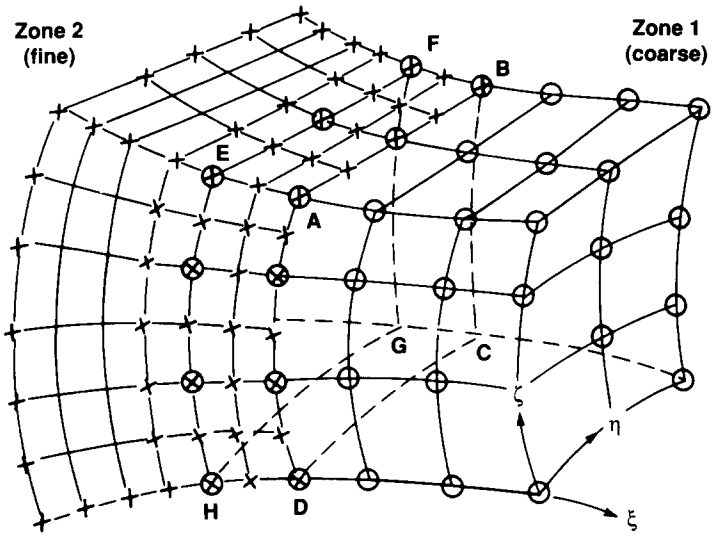

(a) Two-zone grid showing overlap at ABCD and EFGH planes in physical space

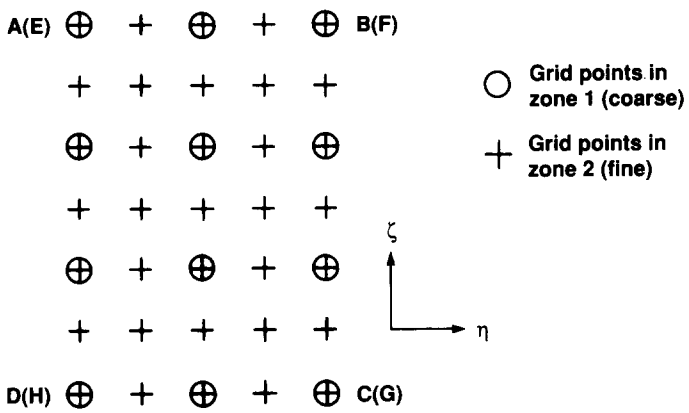

(b) Grid point detail in the overlap region in transformed space

Fig. 3. Grid point details in the zonal interface region.

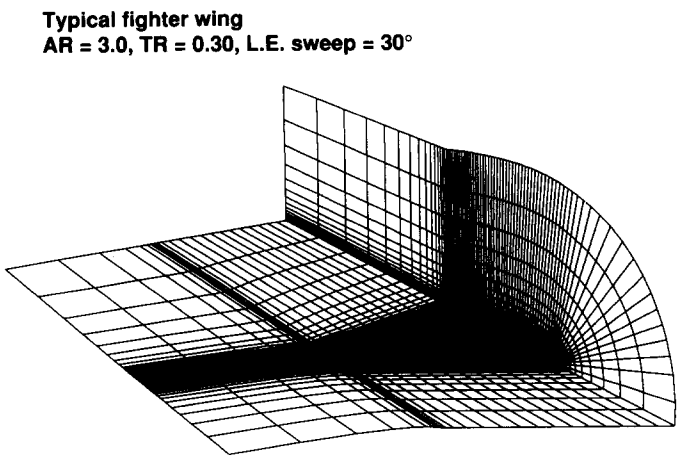

Fig. 4. C–H-type grid for a typical fighter wing.

spacing is small near the wing and stretches exponentially to the outer boundaries. The grid near the leading edge is made finer than the rest of the wing in order to model the geometry accurately. In the spanwise direction, a uniformly distributed grid spacing is used on the wing. To model the wing tip, a finer grid spacing is used. Away from the wing tip, the η grid spacing stretches exponentially. The ζ grid spacing is computed at each time step using the deformed shape of the wing computed using Eq. (5). The ζ grid lines start normal to the surface in the chordwise direction and their spacing stretches exponentially to a fixed outer boundary. To prevent the outer boundaries from moving, the grid is sheared in the ζ direction. The metrics required in the computational domain are computed using the following relations

$$\begin{aligned}\xi_t &= -x_\tau\,\xi_x - y_\tau\xi_y - z_\tau\xi_z\\ \eta_t &= -x_\tau\eta_x - y_\tau\eta_y - z_\tau\eta_z\\ \zeta_t &= -x_\tau\zeta_x - y_\tau\zeta_y - z_\tau\zeta_z.\end{aligned} \tag{8}$$

The grid velocities x_τ, y_τ, and z_τ required in Eq. (8) are computed using the grids at new and old time levels. This adaptive grid-generation scheme is incorporated in ENSAERO. The ability of this scheme to compute accurate aeroelastic responses has been demonstrated in Ref. 8. Figures 5 and 6 illustrate the configuration adaptive grids computed for a rectangular wing undergoing forced bending–torsion motion.

Currently it is assumed in the code that only the grids in the zones attached to the surface are allowed to move. The grid movements approach zero near

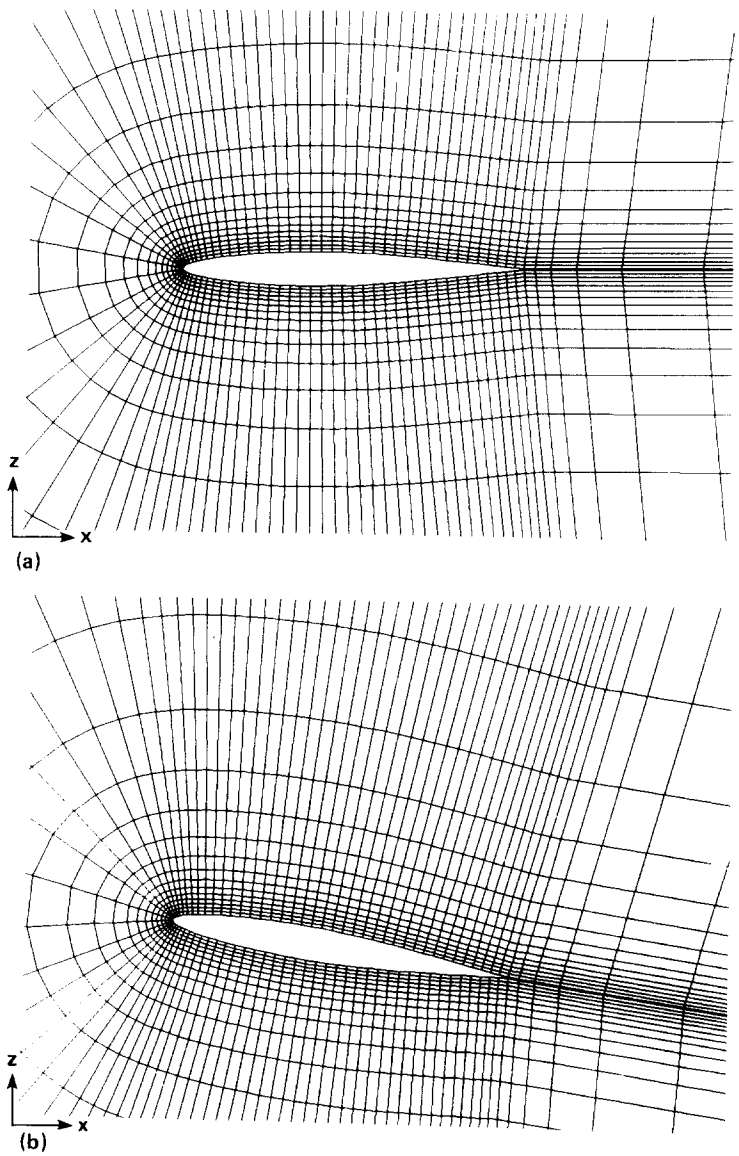

Fig. 5. Chordwise view of grid in x–z plane at 50% semispan location: (a) initial position, and (b) deformed position.

the zonal outer boundaries that interface with other zones. This assumption minimizes errors caused by the moving zonal interfaces.

Computational efficiency and robustness of the solution method are important for CPU time-intensive aeroelastic calculations with configuration-adaptive grids. Therefore, a numerically efficient diagonal algorithm is used. The diagonal algorithm computes time-accurate calculations in a geometrically nonconservative fashion. Geometric conservation can improve the accuracy of the results for moving grids. However, studies have shown that satisfying geometric conservation has little effect on the solutions associated with moving grids. The time steps used for Navier–Stokes calculations are typically small enough that the error from geometric nonconservation is negligible for most practical purposes.

The validation of computed results with experiments reported in this paper and in Ref. 17 further supports the use of the diagonal scheme for computations associated with moving grids. In order to maintain the efficiency and robustness of the diagonal scheme, the present time-accurate computations are made in a geometrically nonconservative fashion.

CODE DESIGN

Computational methods and computer hardware are continually evolving, growing technologies. Modular coding procedures and hardware independence can minimize software maintenance cost,

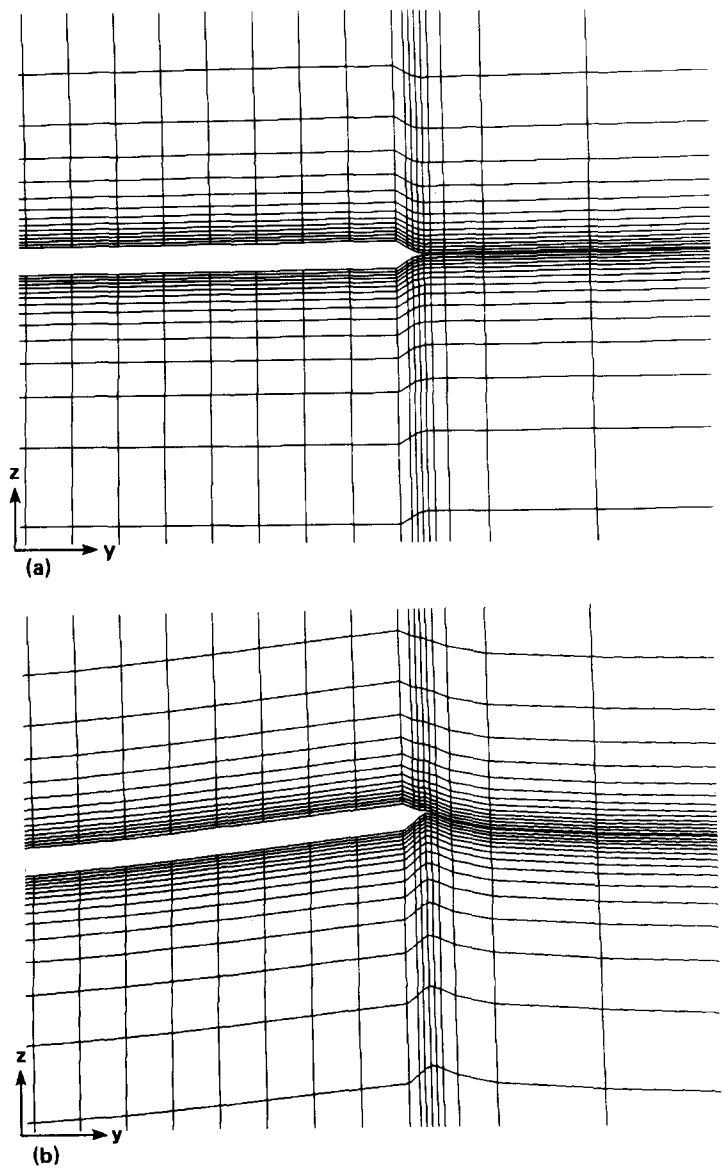

Fig. 6. Spanwise view of grid in y–z plane at 50% chord location: (a) initial position, and (b) deformed position.

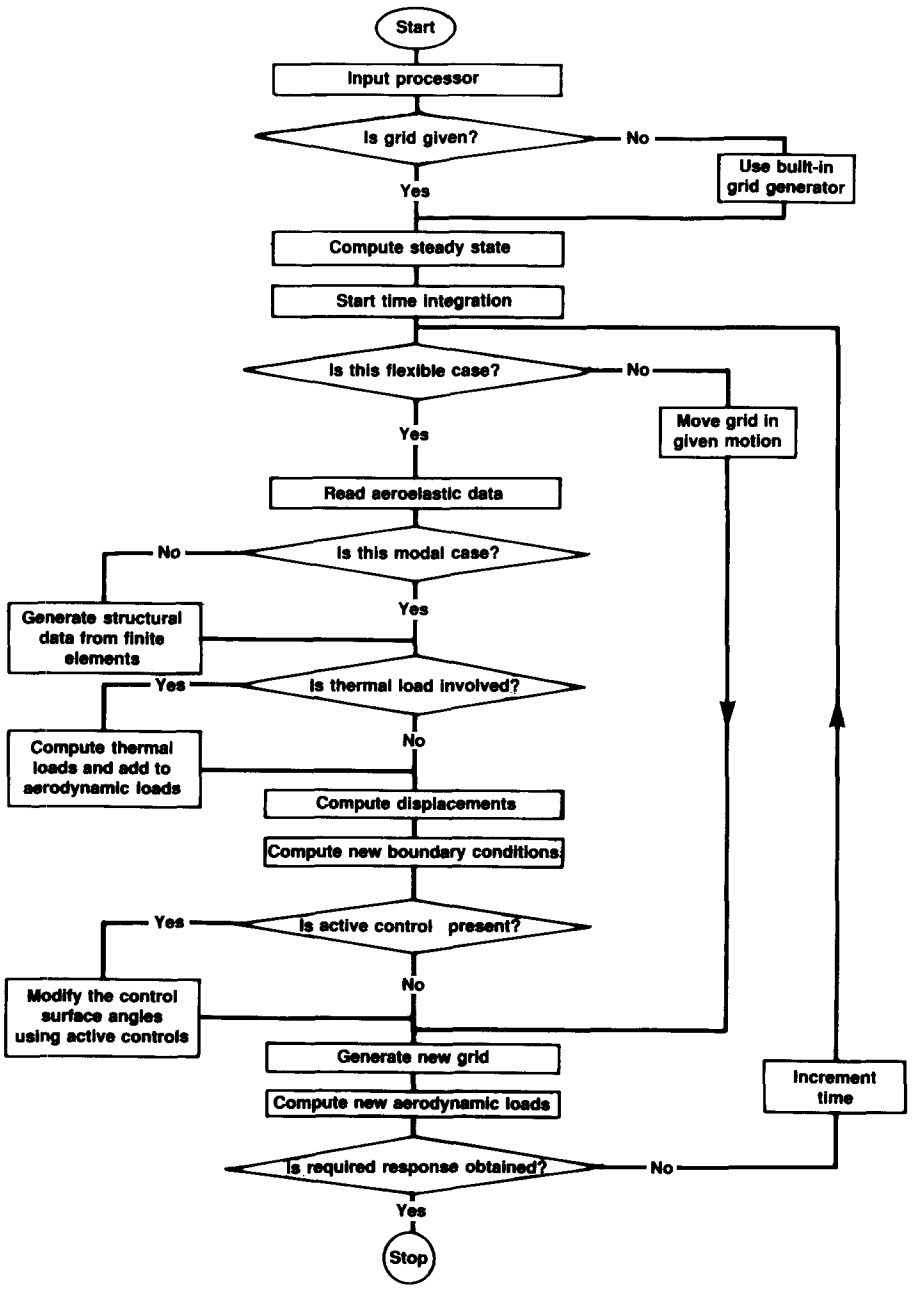

Fig. 7. Flow diagram of ENSAERO.

particularly for multidisciplinary codes. NASTRAN, one of the successful codes of NASA for structural analysis, is a typical example of highly modular coding. Similar efforts have been made for codes based on CFD. ATRAN3S of NASA Ames Research Center[5] is a hardware-independent code written in modular fashion and has been successfully used for multidisciplinary research involving fluids/structures/active controls. However, several issues, such as grids, were simple in ATRAN3S because of the use of the small disturbance equations.

ENSAERO is being designed as a multidisciplinary code. For portability it is written in standard Fortran. It contains eight main modules, namely: (1) Input Processor, (2) Grid Generation, (3) Flow Solver, (4) Finite Elements Structures, (5) Aeroelastic Solution, (6) Active Controls, (7) Thermal Loads, and (8) Post Processor. Each module is independent of others for the purposes of code development and adding new features. The communication between modules takes place only through COMMON BLOCK data. An automated bookkeeping utility, UPDATE, that is available on most of the super computers such as CDC7600, CRAY-YMP, etc., is utilized in programming, This computerized bookkeeping technique is highly

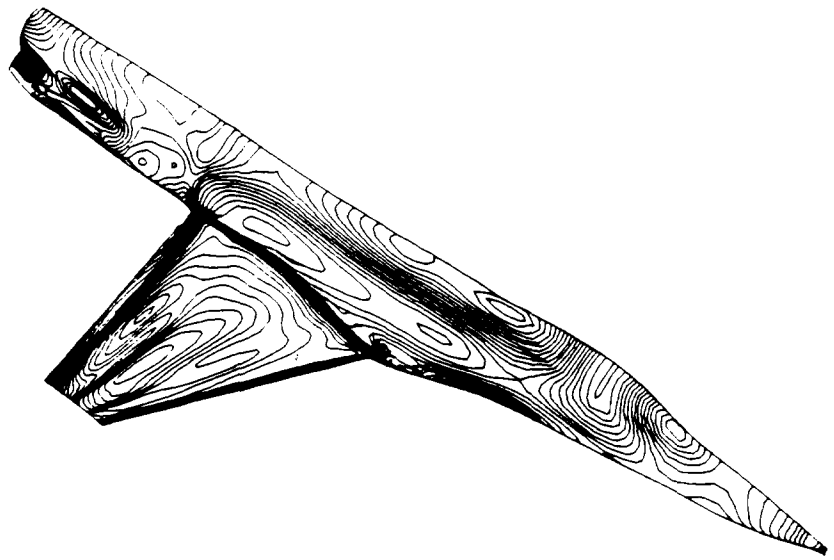

Fig. 8. Mach contours of a typical wing–body configuration at $M = 0.90$, $\alpha = 1.69°$ and $\mathrm{Re} = 4.5 \times 10^6$.

suitable for the multiprogrammer environment of writing large scientific codes. Such an environment is essential for multidisciplinary code development since several analysts and programmers from different disciplines need to mutually coordinate. A flow diagram of the code is illustrated in Fig. 7.

Currently the code is being developed on CRAY-YMP computers available at Ames and Numerical Aerodynamic Simulation (NAS). The current version 2.0 of ENSAERO runs at 130 million floating point operations per second (MFLOPS). The CPU time per time step per grid point is 15×10^{-6} s, and the memory required per grid point is about 30 words with the use of a secondary storage, solid state device (SSD). The memory required per grid point can be further reduced by using the zonal grids in the code.

ILLUSTRATIONS

In this section, some results from ENSAERO are shown to illustrate its various capabilities. Most of the multidisciplinary results illustrate the coupling between flow and structures. All flow computations are made using the central difference option of the code. Unless otherwise stated, all results are presented for turbulent flows.

Steady pressures

The steady-state option of the present development is the same as the TNS code capability with zonal grids.[13] Currently, for steady-state computation, the code can model full aircraft such as the F-16. Figure 8 illustrates the steady-pressure contours on the F-16 aircraft by using 27 zones. The capability of the code to compute separated flows has already been demonstrated.[13] The capability of the code to compute flows at moderate high angles of attack is illustrated in Fig. 9 by computing the lifts up to 20° angle of attack for a delta wing.

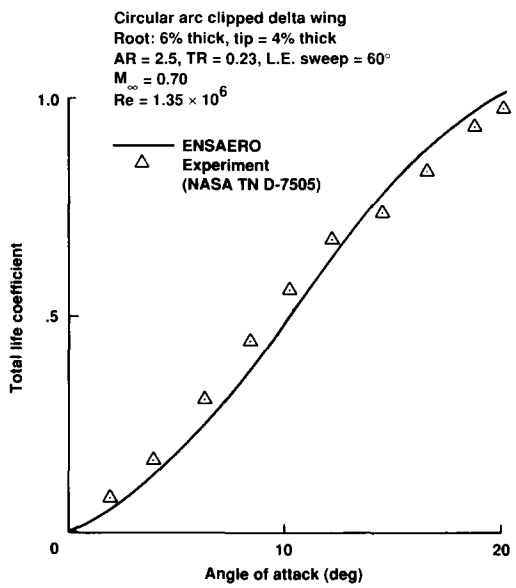

Fig. 9. Comparison of computed lifts with the experiment.

Unsteady pressures on rigid wings in oscillating motion

ENSAERO has an option of computing unsteady flows over wings in oscillating and ramp motions. In the code, efficient procedure is provided to switch between Euler and Navier–Stokes equations. Figure 10 shows the Euler and Navier–Stokes unsteady pressures on the AGARD rectangular wing in a pitching motion. The wing is pitching about the mid-chord with a reduced frequency k based on a root chord equal to 0.27. The Navier–Stokes results

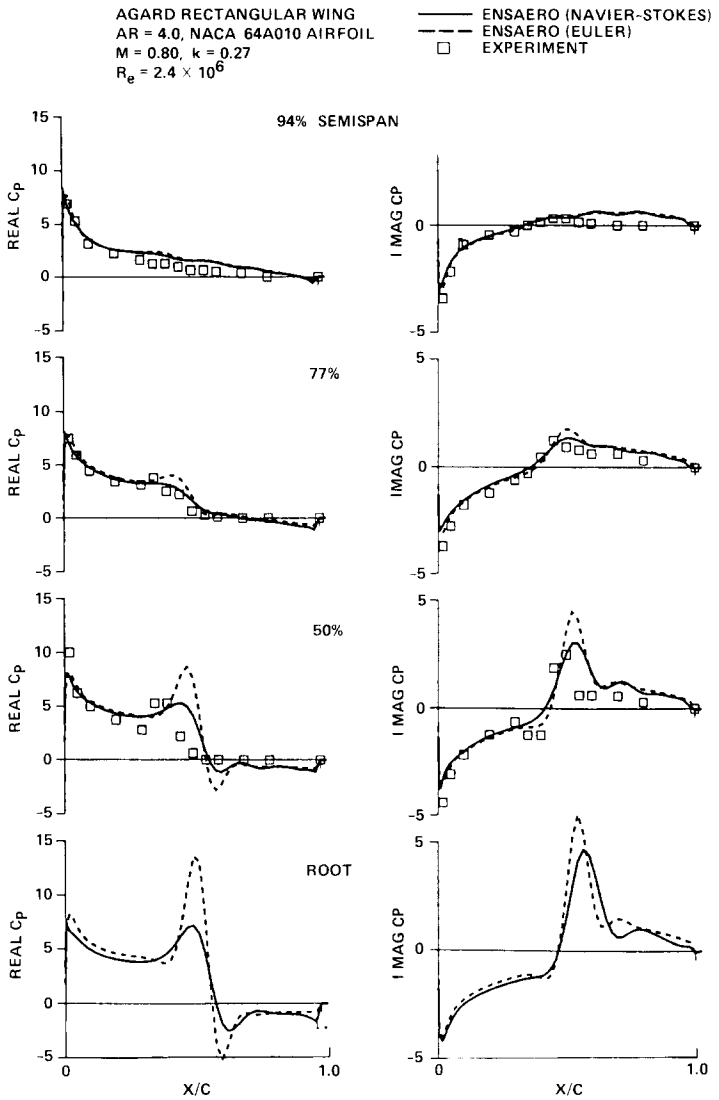

Fig. 10. Comparison of Euler and Navier–Stokes unsteady pressures with the experiment.

compare better with the experiment than do the Euler results.

The present code has an important capability for zonal grids which was earlier developed for the steady-state computations. This zonal grid capability is extended for moving grids.[17] Figure 11 illustrates the two-zone computation on the AGARD rectangular wing in pitching motion. The smooth variation of Mach contours through the zonal interface can be seen in the figure. This illustrates the potential of the present code to treat complete geometry with moving zonal grids.

The geometry capability in the code can handle general wing motions. This is illustrated by computing the unsteady pressures over the F-5 wing oscillating in a pitching mode, as shown in Fig. 12. The unsteady pressures at subsonic Mach number are shown in Fig. 13.

Unsteady pressures on rigid wings in ramp motion

In this section, ENSAERO is demonstrated to compute flow over a typical fighter wing pitching from $\alpha = 0.0$ to 30.0° in a ramp motion. The wing selected has an aspect ratio of 3.0, a taper ratio of 0.30 and a leading-edge sweep angle of 30° with NACA0015 sections. Laminar flow computations are made on both rigid and flexible configurations. All computations for both the rigid and flexible wings are made for $M_\infty = 0.50$ and $\mathrm{Re}_c = 2.0 \times 10^6$, using a time-step size of 8.4×10^{-3}. From numerical experiments, it was found that the time-step size used was adequate to obtain a stable and accurate unsteady solution.

For the rigid wing, computations were made at three pitch rates (A): 0.10, 0.050, and 0.025. The pitch rate, A, is defined as $\dot{\alpha}c/U_\infty$, where α is measured in radians. Figure 14 shows computed

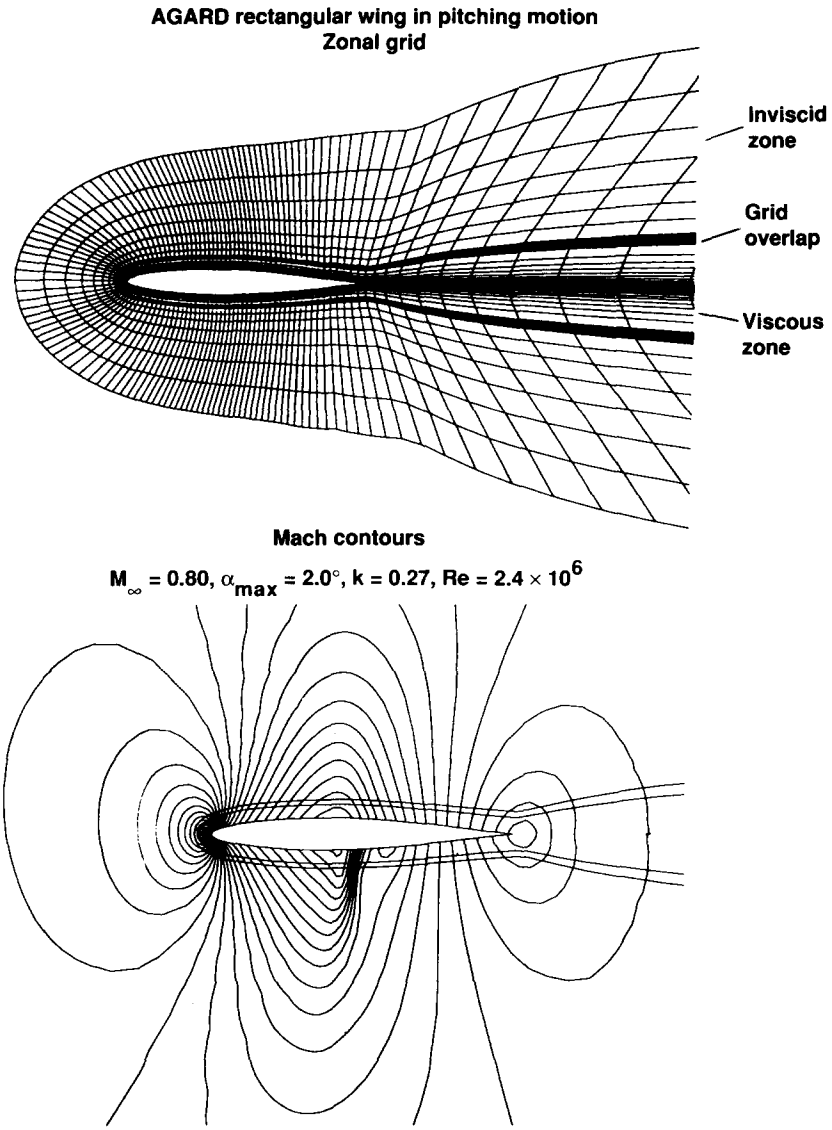

Fig. 11. Mach contours at 50% semispan station using two–zone grid for an oscillating wing.

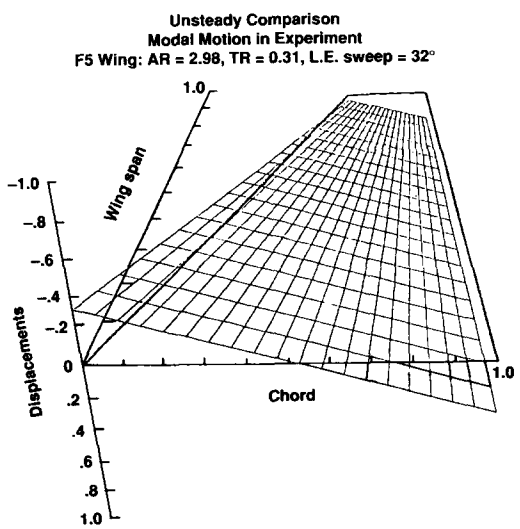

Fig. 12. Unsteady motion of a rigid fighter wing.

responses of upper surface unsteady pressures for the rigid wing undergoing a ramp motion from $\alpha = 0.0$ to 30° at a pitch rate of 0.1. For this pitch rate, the wing reaches $\alpha = 30°$ at a nondimensional time of 10.47 as indicated by the arrow in Fig. 14. Chordwise pressure histories for spanwise stations located at $2y/b = 0.0$, 0.3, 0.6, and 0.9 are shown in Fig. 14a–d, respectively. The unsteady computations are started from a converged steady-state solution at $\alpha = 0.0°$. Figure 14 also shows the vortex wing interaction due to initiation, development, and convection of the leading-edge vortex using three-dimensional pressure topologies plotted at four span stations. The results in Fig. 14 show the dynamics of vortex development. As the wing is pitched toward the maximum angle of attack, a rapid pressure decrease (increasing suction peak) occurs over the leading edge, which signals the formation of a leading-edge vortex. This vortex starts moving downstream

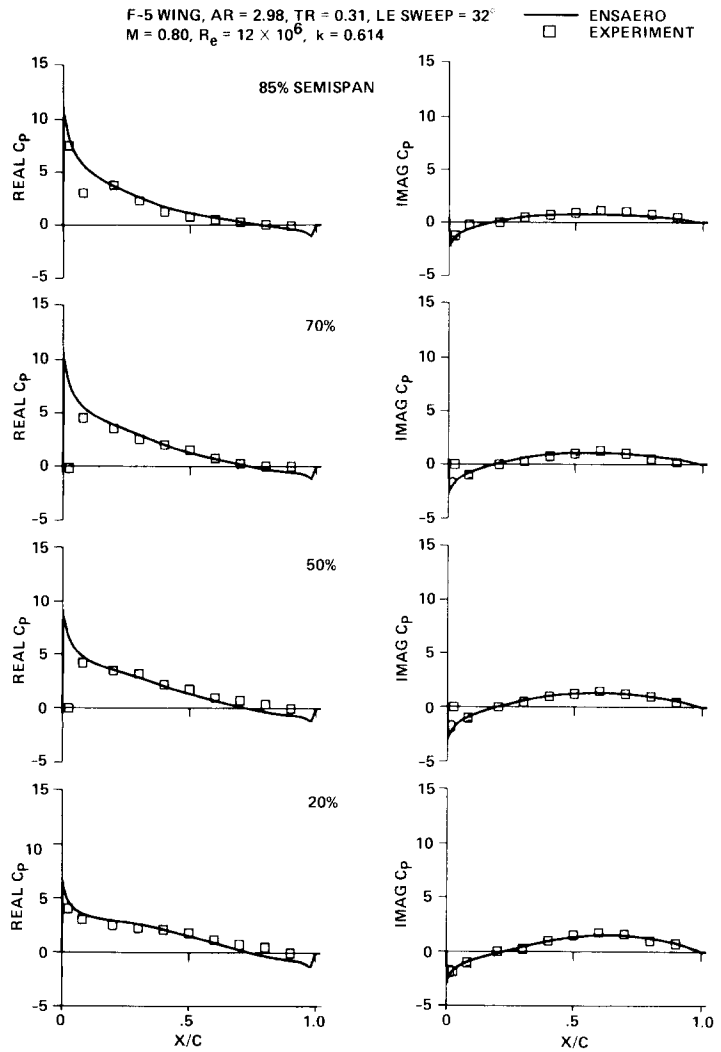

Fig. 13. Comparison of the Navier–Stokes unsteady pressures with the experiment for a typical fighter wing.

rapidly after the wing has reached a certain angle of attack. The vortex motion is highly three-dimensional. The vortex core starts moving downstream earlier for span stations closer to the tip. Also, it is observed that the tip stall occurs before the root stall. This computation requires about 5 h of CPU time on a CRAY-YMP832 computer.

One area where unsteady vortical flows play an important role is in increasing the dynamic lift. From earlier studies on airfoils, it has been observed that the dynamic lift can be increased by increasing the pitch rates. It is expected that such increases in the dynamic lift can be used in maneuvering an aircraft.[18] Because the dynamic lift is an unsteady phenomenon and is associated with the presence of vortices, it is important to model it accurately. The present computational tool is used to investigate dynamic lift over fighter wings, including the wing flexibility. Computations are made for the rigid fighter wing for pitch rates $A = 0.05$ and 0.025, and the results are compared with those obtained earlier for $A = 0.10$. The unsteady lift is plotted against time (in degrees) in Fig. 15. Thus the wing reaches the maximum value $\alpha = 30°$ at t (in degrees) = 30. For all pitch rates, the stall occurs at the wing tip before it occurs at the root section. The increase in the dynamic lift at the higher pitch rates can be seen in Fig. 15.

As stated in the Introduction, it is important to account for the flexibility of the wing. Significant details of physics may be lost if the wing flexibility is neglected. To illustrate the importance of the wing flexibility, computations are made on a flexible configuration of the fighter wing. The structural properties of the flexible wing are modeled using four modes. The mode shapes and frequencies of the first four modes computed using the finite element method are shown in Fig. 16. These modes and frequencies represent the structural properties of a typical fighter wing. Aeroelastic computations are made at a dynamic pressure of 0.5 psi.

The same computations made on the rigid wing are also made on the flexible wing. Figure 17 shows the

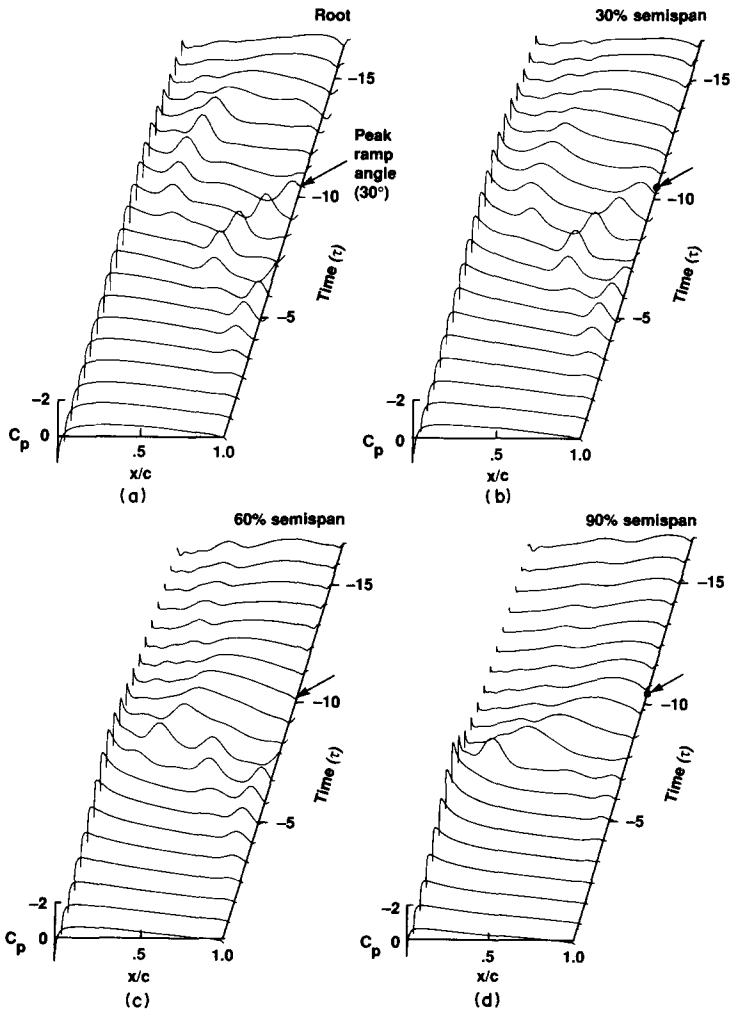

Fig. 14. Unsteady surface pressure responses of a rigid fighter wing in ramp motion.

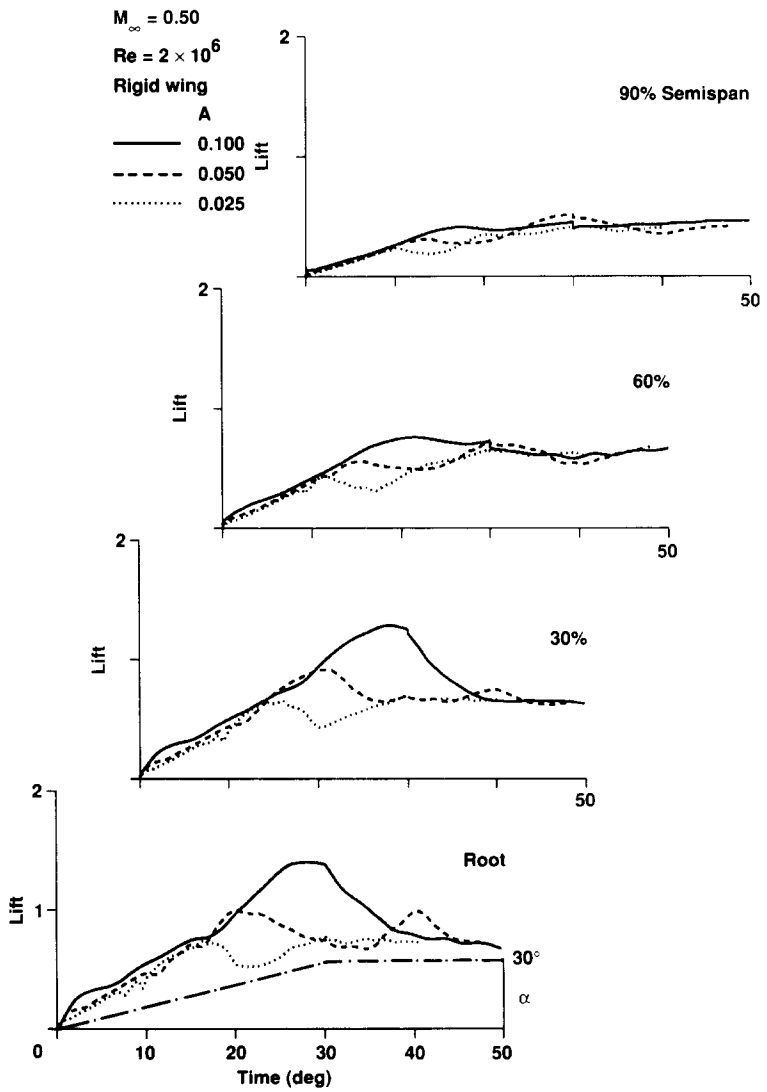

Fig. 15. Unsteady lift responses of a rigid fighter wing in ramp motion.

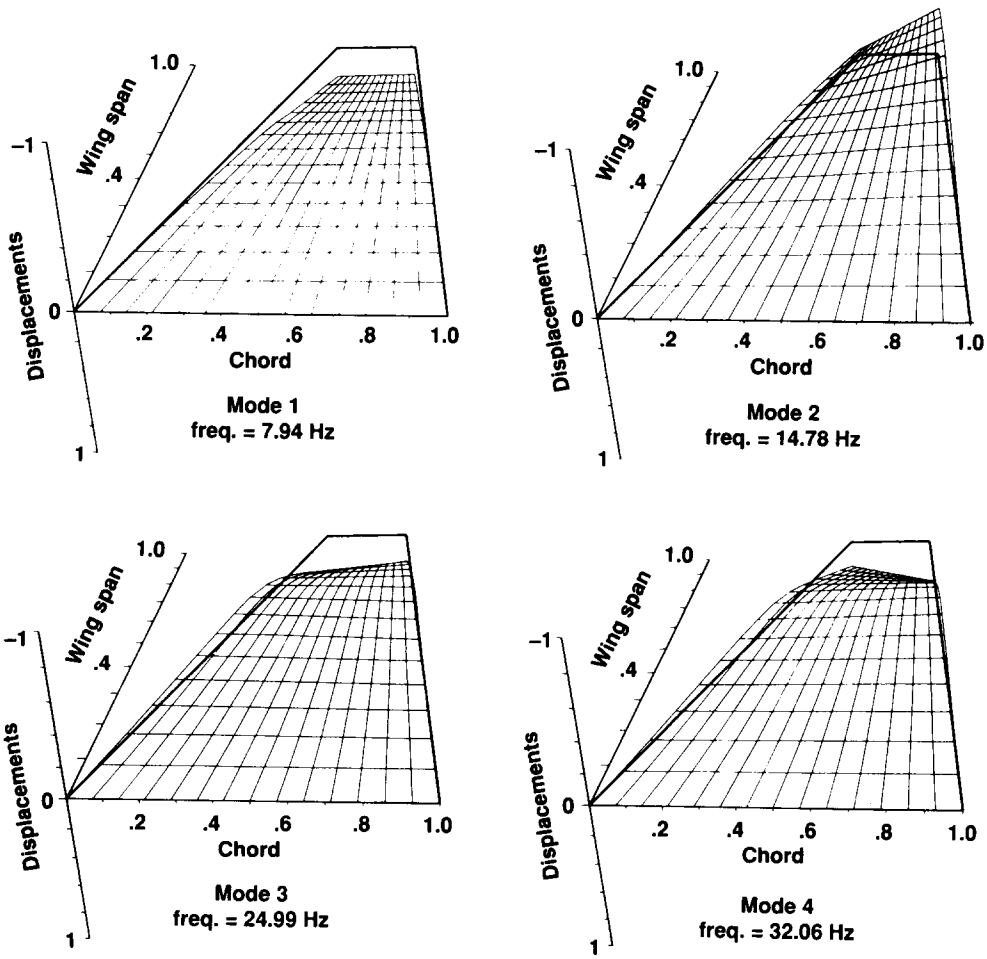

Fig. 16. Mode shapes of a typical flexible fighter wing.

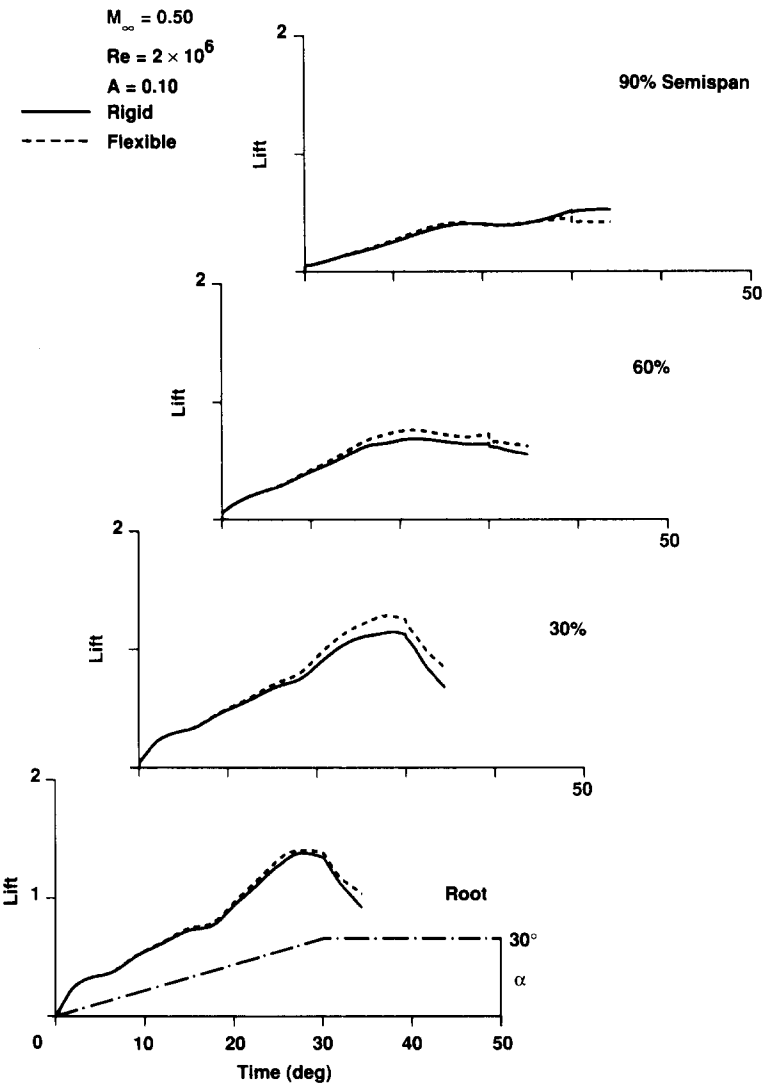

Fig. 17. Comparison of lift responses between rigid and flexible wings in ramp motion.

unsteady sectional-lift coefficients plotted against time for both the rigid wing and the flexible wing. At a given time, the lift over the flexible wing is higher than the lift over the rigid wing. This is due to the increase in the angle of attack caused by the wing flexibility. The deformed shape of the wing and the velocity contours in the free-stream direction are shown in Fig. 18. The convection of the leading-edge vortex can also be seen in Fig. 18.

Wings with active controls

The present development can be used for computing aeroelastic responses of aircraft with active controls. The active control module developed by the present author for ATRAN3S[5] is used in this work. Figure 19 illustrates the use of active controls to suppress the aeroelastic oscillations by using the small perturbation theory. More details of this work can be found in Ref. 19.

CONCLUSIONS

In this paper, a computational procedure for multidisciplinary computations involving fluid/structural interactions is presented. The present development uses a moving zonal grid concept to model complex flexible aerospace vehicles. The flow is modeled using the Euler/Navier–Stokes equations, and computations are made using efficient methods based on both central and upwind schemes. The structure is represented by a finite element method which can model general aerospace vehicles. Provisions are made to accommodate other disciplines such as controls and thermal loads. The capability of the code to compute unsteady flows on flexible wings with vortical flows is demonstrated. The present development is a useful computational tool for the multidisciplinary area involving fluid/structural interactions and can be extended to include controls and thermal loads. Adaption of this computational

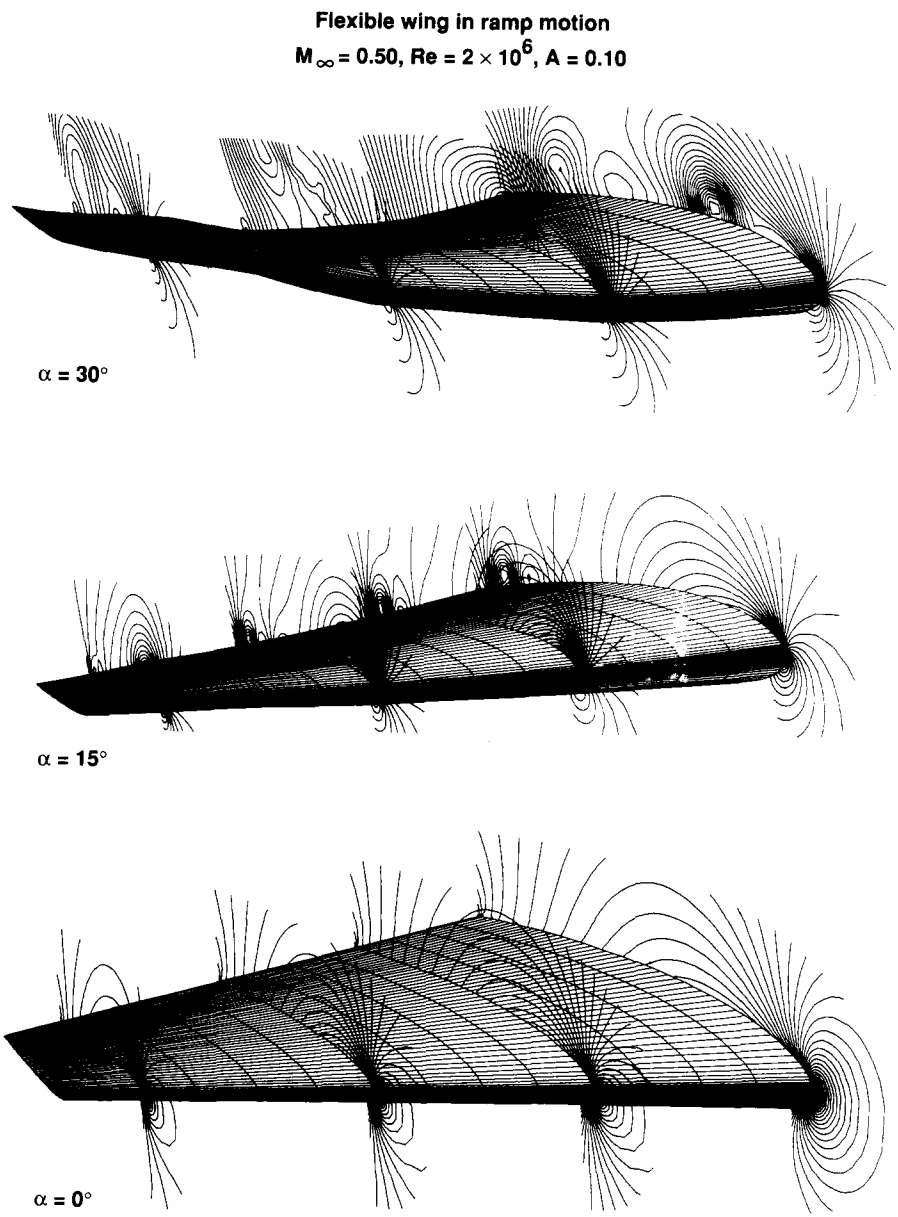

Fig. 18. Unsteady pressure contours over the flexible wing in ramp motion.

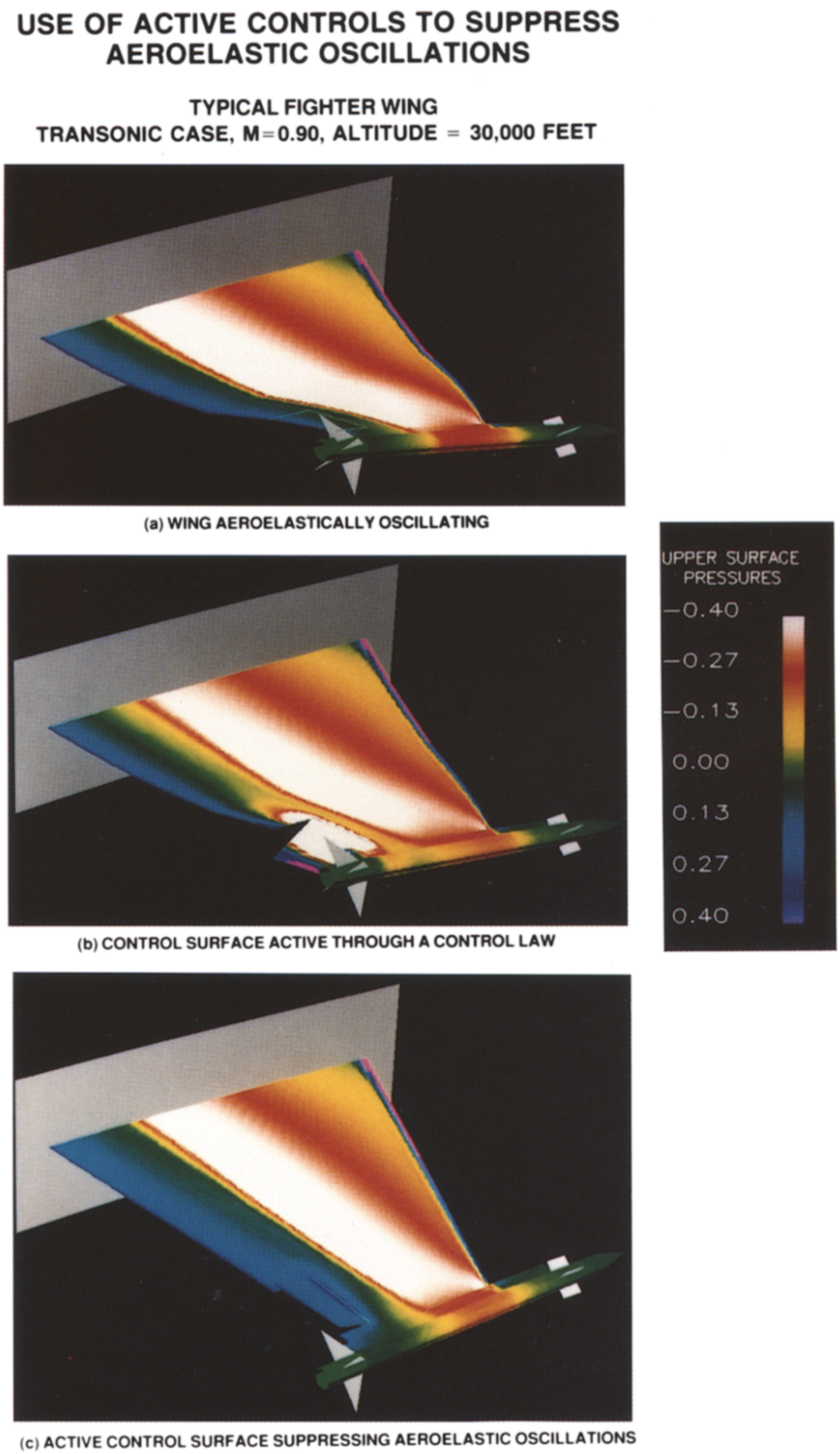

Fig. 19. Active controls suppressing aeroelastic oscillations.

tool for parallel processing and validation for complete aerospace configurations is in progress.

REFERENCES

1. S. K. Dobbs, G. D. Miller and J. R. Stevenson, "Self-induced oscillation wind tunnel test of a variable sweep wing," AIAA 85-0739-CP, 1985.
2. G. P. Guruswamy, P. M. Goorjian, H. Ide and G. D. Miller, "Transonic aeroelastic analysis of the B-1 wing," *Journal of Aircraft* **23,** 547–553 (1986).
3. M. G. Farmer and P. W. Hanson, "Comparison of supercritical and conventional wing flutter characteristics," NASA TM X-72837, 1976.
4. H. Ashley, "Role of shocks in the sub-transonic flutter phenomenon," *Journal of Aircraft* **17,** 187–197 (1980).
5. G. P. Guruswamy, "Integrated approach for active coupling of structures and fluids," *AIAA Journal* **27,** 788–793 (1989).
6. G. P. Guruswamy and E. L. Tu, "Transonic aeroelasticity of fighter wings with active control surfaces," *Journal of Aircraft* **26,** 682–684 (1989).
7. T. A. Edwards and J. Flores, "Towards a CFD nose-to-tail capability: hypersonic unsteady Navier–Stokes code validation," AIAA-89-1672, 1989.
8. G. P. Guruswamy, "Unsteady aerodynamics and aeroelastic calculations for wings using Euler equations," *AIAA Journal* **28,** 461–469 (1990).
9. G. P. Guruswamy, "Navier–Stokes computations on swept-tapered wings, including flexibility," AIAA-90-1152-CP, 1990.
10. R. Beam and R. F. Warming, "An implicit finite difference algorithm for hyperbolic systems in conservation-law form," *Journal of Computational Physics* **22,** 87–110 (1976).
11. T. H. Pulliam and D. S. Chaussee, "A diagonal form of an implicit approximate factorization algorithm," *Journal of Computational Physics* **39,** 347–363 (1981).
12. S. Obayashi and P. M. Goorjian, "Improvements and applications of a streamwise upwind algorithm," AIAA-89-1957, 1989.
13. J. Flores, "Simulation of transonic viscous wing and wing-fuselage flows using zonal methods," NASA TM-89421, 1987.
14. B. S. Baldwin and H. Lomax, "Thin layer approximation and algebraic model for separated turbulent flows," AIAA-78-257, 1978.
15. G. P. Guruswamy and T. Y. Yang, "Aeroelastic time response analysis of thin airfoils by transonic code LTRAN2," *Computers and Fluids* **9,** 409–425 (1980).
16. T. Y. Yang, *Finite Element Structural Analysis*, Prentice–Hall, Englewood Cliffs, NJ, 1986.
17. N. Chaderjian and G. P. Guruswamy, "Unsteady transonic Navier–Stokes computations for an oscillating wing using single and multiple zones," AIAA paper 90–0313, 1990.
18. D. G. Mabey, "On the prospects for increasing dynamic lift," *Aeronautical Journal of the Royal Aeronautical Society* 95–105 (1988).
19. G. P. Guruswamy and E. L. Tu, "Transonic aeroelasticity of fighter wings with active control surface," *Journal of Aircraft* **26,** 682–684 (1989).